ADVANCED FUNCTIONAL MATERIALS
www.afm-journal.de

Enhancing the Photocatalytic Activity via Direct Covalent Functionalization in Single-Walled Carbon Nanotubes

José Luis Nova-Fernández, Daniel González-Muñoz, Gustavo Pascual-Coca, Mattia Cattelan, Stefano Agnoli, Raúl Pérez-Ruiz, José Alemán, Silvia Cabrera,* and Matías Blanco**

Herein, the direct covalent functionalization of single-walled carbon nanotubes (SWNT) is presented with an amino-decorated phenyl-phenothiazine (PTH-NH_2) organophotocatalyst through the diazonium chemistry protocol. Three different SWNT-PTH hybrids are prepared by varying the amount of PTH-NH_2 and diazonium agent and are fully characterized. These hybrids differ not only in the degree of functionalization, but also in the chemical structure and the photophysical properties. The study shows that these features affect the photoredox activity of the materials in the photo-debromination of aromatic halides. Thus, sample SWNT-PTH-5, a functionalized nanotube with a 5% wt loading of PTH, surpasses the catalytic performance of homogeneous PTH in 11 different substrates, finishing the reaction in shorter times, in a recyclable manner and without catalyst leaching. This study demonstrates the importance of controlling the functionalization degree of SWNT with photocatalysts to prepare photocatalytic materials with even higher catalytic activity than that presented by the homogeneous PTH catalyst.

1. Introduction

Photoredox catalysis mediated by visible light has received much attention during the past decades.[1–4] Its mild and "green" conditions have made photoredox catalysis a suitable option in the development of new efficient, economical and environmentally friendly transformations. In the field of organic synthesis, organic dyes are one of the best options for photocatalytic applications, due to their easy preparation and low cost.[5] However, some of them suffer degradation under the reaction conditions and present low solubility in aqueous solutions and common organic solvents due to the pseudo-planarity of the organic catalyst (**Scheme 1a**). This is the case of 10-phenylphenothiazine (PTH), which is a highly reducing organic photocatalyst [E° ($PTH^{\bullet+}$/PTH*) = −2.1 V vs

J. L. Nova-Fernández, D. González-Muñoz, J. Alemán, M. Blanco
Organic Chemistry Department
Universidad Autónoma de Madrid
Madrid 28049, Spain
E-mail: jose.aleman@uam.es; matias.blanco@uam.es
J. L. Nova-Fernández, G. Pascual-Coca
Synthelia Organics Labs
C/ Torres Quevedo 15, Alcobendas 28108, Spain
M. Cattelan, S. Agnoli
Department of Chemical Sciences
Consorzio Interuniversitario Reattività
Chimica e Catalisi (CIRCC)
University of Padova
Via Marzolo, 1, Padova 35131, Italy
R. Pérez-Ruiz
Departamento de Química
Universitat Politècnica de València
Camino de Vera S/N, Valencia 46022, Spain
J. Alemán, S. Cabrera, M. Blanco
Institute for Advanced Research in Chemical Sciences (IAdChem)
Universidad Autónoma de Madrid
Madrid 28049, Spain
E-mail: silvia.cabrera@uam.es
J. Alemán
Center for Innovation in Advanced Chemistry (ORFEO-CINQA)
Universidad Autónoma de Madrid
Madrid 28049, Spain
S. Cabrera
Inorganic Chemistry Department
Universidad Autónoma de Madrid
Madrid 28049, Spain

The ORCID identification number(s) for the author(s) of this article can be found under https://doi.org/10.1002/adfm.202313102

DOI: 10.1002/adfm.202313102

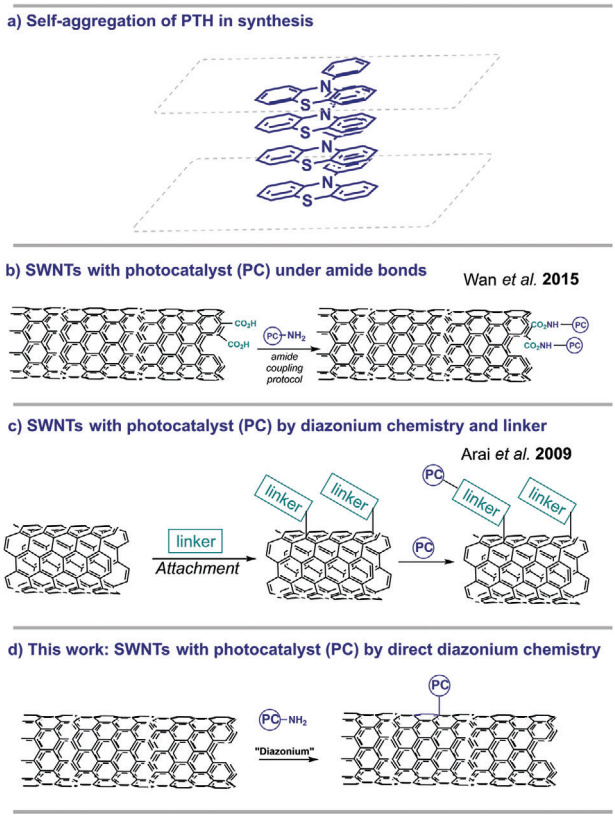

Scheme 1. a) Self-aggregation of homogeneous photocatalysts; b,c) diverse strategies reported for the incorporation of photocatalysts in nanotubes compared to d) the present work.

SCE; $E°$ ($PTH^{\bullet+}/PTH$) = 0.68 V vs SCE][6,7] with a great ability for the reduction of carbon-halogen bonds.[7] Although the molecule is easy to synthesize and its employment as photocatalyst supposes a low-cost treatment,[8] it is well-known for its little solubility in organic solvents due to the self-aggregation of the molecule. This fact markedly reduces its photocatalytic activity as a consequence of autoquenching phenomena (Scheme 1a) since the probability of autorelaxation of the excited molecules due to collision inside the aggregate is higher than the efficient electron transfer.[9]

Nowadays, single walled carbon nanotubes (SWNT) have been established as an excellent platform for the development of efficient nanomaterials with photocatalytic properties.[10] Their unique electronic, conductive, and mechanical properties, as well as their stability, robustness and high surface area are essential for their excellent and wide applicability in the catalytic field.[11,12] In addition, combined with photoactive motifs, SWNT are able to assist in the photoinduced electron-transfer phenomena due to their outstanding electron-storage capacity, for example, by accepting excited photoelectrons in their π system, thus delaying the recombination process.[10,13–16] Therefore, SWNT-based hybrids have started to be prepared for photocatalysis using different strategies. The first and most common is the functionalization of the open edges or the sidewalls of the SWNT by covalent attachment, which includes the formation of an amide (or ester) bond between the amino (or alcohol) functionalized photocatalyst and the acids of the nanotube (Scheme 1b).[17] This straightforward methodology presents as main limitation the location of all the photocatalytic molecules in the same region of space, i.e., the SWNT edges, which would lead to quenching phenomena due to the proximity of the photocatalytic units to each other.[18,19] Another approach reported in the literature is the incorporation of the photocatalytic unit into the structure of the nanotube through a linker.[20–25] This stepwise approach first involves the incorporation of the linker to the nanotube structure using different organic reactions such as cycloadditions, diazonium chemistry and/or amide couplings among others. Next, the photocatalyst with the adequate reactive moiety, whose derivatization typically requires additional synthetic steps, is covalently bonded to the linker (Scheme 1c). However, the incorporation of the catalyst to the nanotube is not maximized since not all the linkers react. Although this approach may avoid the phenomenon of autoquenching through separation of the active centers, it generates an excess of sp^3 carbons and other defects in the nanotube structure which might hinder the photocatalytic performance.[26–28] In addition, the design of the linker, in terms of its length and structure, is key to avoid the loss of the electronic communication between both units, i.e., the photocatalyst and the nanotube (generally aliphatic linkers are employed, which break electronic communication).[21] Moreover, the presence of the linker implies increasing the distance between the photoactive unit and the nanotube core, which may result in detrimental effects for an eventual catalytic application, combined with the potential nanotube damage due to the multistep procedure. Indeed, it is widely accepted that the photocatalytic activity of the photocatalyst-linker-SWNT hybrids is due to the development of efficient photoinduced charge transfer phenomena between the two species, i.e., dye and SWNT.[21,29,30] For example, zinc porphyrin-linker-SWNT hybrids have been reported, in which the incorporation of the SWNT provoked an enhancement of the absorption capacity and in their photocatalytic performance toward the degradation of pollutants compared with the unsupported porphyrin.[17] These kind of studies showed the extra features of the heterogeneous SWNT-based photocatalyst over the parent homogeneous catalyst, due to the synergistic effect of both entities in the hybrid. Despite such effects, the study and application of other photocatalytic hybrids prepared by covalent binding of the SWNT and common organic photocatalysts has received less attention.

Therefore, the direct binding of the photocatalyst to the carbon scaffold of the SWNT, using diazonium chemistry and aromatic amines, without the use of a linker or any other functionalization step, could provide a direct and straightforward solution to functionalize the nanotube surface with the photoactive dye (Scheme 1d). Bearing all these considerations in mind, in this work we present the preparation and characterization of SWNT-PTH hybrids using diazonium chemistry with the aim of reducing the aggregation issues of PTH in solution as well as improving the photocatalytic performance of the homogeneous organophotocatalyst. To the best of our knowledge, this is the first time that an organic photocatalyst has been directly attached to the SWNT core, avoiding any distance between them, without the insertion of any spacer/linker. Furthermore, the SWNT-PTH hybrids are synthesized with different PTH content for comparative purposes. Such hybrids will combine the electron mobility and charge transfer ability of SWNT with the photoredox properties

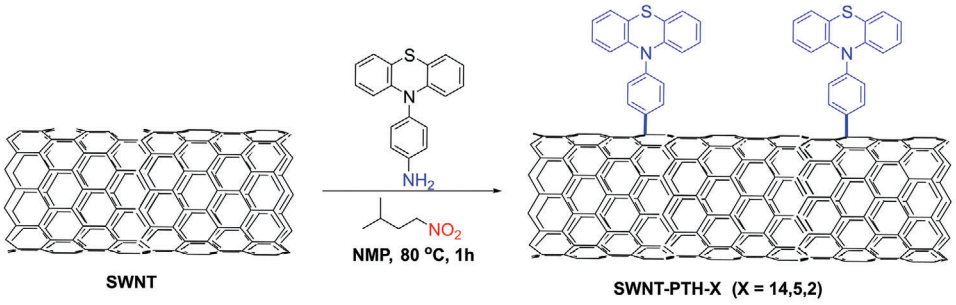

EXPERIMENT	PTH-NH_2	Isoamyl nitrite	SWNT-PTH-X
EXPERIMENT 1	0.3 mmol	0.6 mmol	**SWNT-PTH-14**
EXPERIMENT 2	0.03 mmol	0.06 mmol	**SWNT-PTH-5**
EXPERIMENT 3	0.003 mmol	0.006 mmol	**SWNT-PTH-2**

Scheme 2. Covalent decoration of the nanotubes with the PTH catalyst via the diazonium chemistry protocol (X denotes the PTH functionalization in % wt).

of PTH.[31,32] Their catalytic performance is evaluated for different photoredox reactions,[33] showing the outstanding activity of these new photocatalytic materials.

2. Results and Discussion

2.1. Synthesis of the Hybrid Catalyst

Initially, commercial single walled carbon nanotubes (SWNT) of 1.4 nm diameter and several μm in length were subjected to a wet acid treatment.[24,25,34,35] This treatment, as demonstrated by the characterizations performed (see Supporting Information, for further details), was able to eliminate all the impurities such as amorphous carbon or the metals used for the synthesis of the nanotubes, yielding purified **SWNT**. Following this procedure, the nanotubes were very clean (we did not find objects surrounding the tube after exhaustive TEM observations) with a preserved carbon structure, (see TEM Figure S2, Supporting Information), the metals were removed (see TXRF Figure S3, Supporting Information), but the chemical composition showed an oxygen content of 16% wt (see elemental analysis, **Table 1**). To accomplish the covalent functionalization of the SWNT with PTH, the catalyst was modified to provide an adequate functionalization for its bonding with the nanotube. Thus, **PTH-NH_2** was synthesized through a Buchwald-Hartwig cross-coupling reaction between phenothiazine and 1-bromo-4-nitrobenzene,[32] followed by a reduction of the nitro group with hydrazine (see Supporting Information for further details).[36] In addition, **PTH** was also synthesized for comparative purposes (see Supporting Information).[31]

Table 1. Elemental analysis and PTH loading.

Sample	C [% wt]	H [% wt]	N [% wt]	S [% wt]	PTH Loading [% wt]
SWNT	83.1	1.1	0.1	0.1	–
SWNT-PTH-2	82.4	1.2	0.1	0.2	2
SWNT-PTH-5	81.8	1.9	0.9	0.6	5
SWNT-PTH-14	82.1	2.1	1.2	1.6	14

Next, the carbon structure of the purified SWNT was covalently functionalized with **PTH-NH_2** following a diazonium chemistry anchoring protocol. Thus, purified **SWNT**, the aminophotocatalyst **PTH-NH_2**, and isoamyl nitrite were mixed to in situ generate the corresponding diazonium salt PTH-N_2^+.[24,25,37] Heating the reaction mixture provoked the elimination of N_2 gas, generating a radical that is trapped by the aromatic structure of the SWNT nanotube wall (that performs as reactant), thus binding both units by a strong covalent bond (See **Scheme 2**). Moreover, such protocol allows us to control the functionalization degree of the SWNT by adjusting the **PTH-NH_2** and isoamyl nitrite proportion. The quantity of nanotubes added were fixed at 12 mg of black powder. Thus, we prepared a sample named **SWNT-PTH-14** by adding 0.3 mmol of **PTH-NH_2** and 0.6 mmol of isoamyl nitrite. By decreasing 10-fold and 100-fold the amount of **PTH-NH_2** and isoamyl nitrite, the samples **SWNT-PTH-5** and **SWNT-PTH-2**, respectively, were yielded.

The degree of functionalization of the three materials was calculated according to the S content detected by elemental analysis (Table 1). For sample **SWNT-PTH-14**, a 1.6% wt of S was found, which corresponds to a ≈14% functionalization degree considering the PTH molecule. Samples obtained from the treatment of SWNT with lower amounts of **PTH-NH_2**/isoamyl nitrite (experiments 2 and 3, see Scheme 2) showed correspondingly lower PTH loadings. Thus, a 5% functionalization degree was obtained for sample **SWNT-PTH-5** (0.6% wt of S), whereas **SWNT-PTH-2** showed an almost similar S content as that of purified SWNT. In addition, we also detected an increase in the N and H content of the samples (elements present in the PTH molecule), which was proportional to the dose of reactants subjected to the functionalization treatment, and the increase matched the trend discussed for the S content. The extent of the functionalization was cross-checked by TGA, achieving similar amounts of weight loss at 400 °C compared to the elemental analysis (**SWNT-PTH-2** showed a 5% weight loss, **SWNT-PTH-5** exhibited an 8% weight

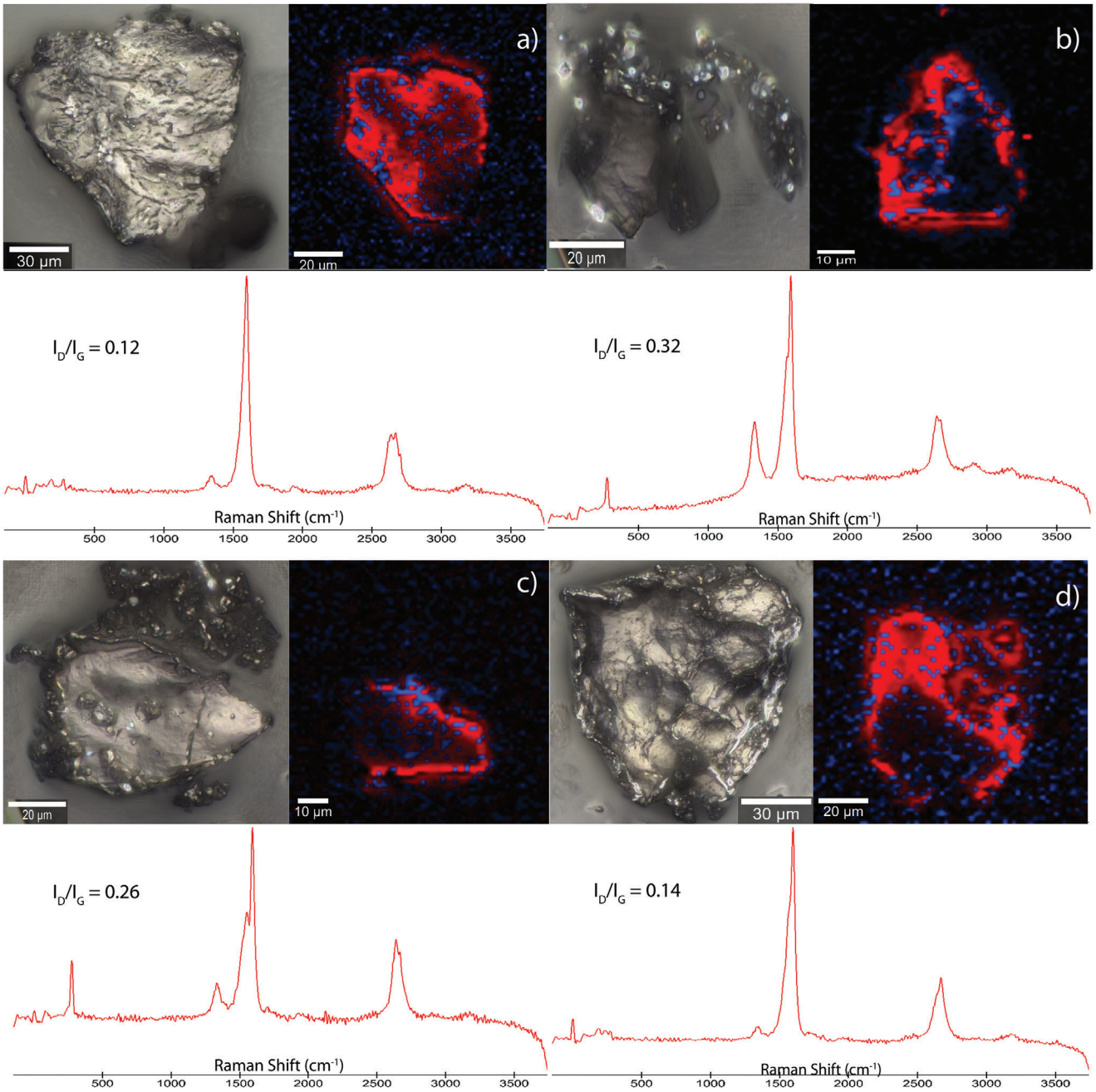

Figure 1. Optical image (grey scale panel), I_D/I_G Raman map (blue-red scale panel) and Raman spectrum (including I_D/I_G ratio) of samples: a) **SWNT**, b) **SWNT-PTH-14**, c) **SWNT-PTH-5**, and d) **SWNT-PTH-2**.

loss, and a 15% loss was observed for **SWNT-PTH-14**, see Figure S4, Supporting Information).

D/IGThe structure of the **SWNT-PTH** functionalized nanotubes was analyzed by Raman spectroscopy and compared to that of purified **SWNT** (**Figure 1**). It was expected that the nanotube structure would be progressively affected according to the increase of the PTH-functionalization degree. First, the Raman spectrum of the purified sample **SWNT** showed the typical Raman pattern of single walled nanotubes, where the radial breathing mode (RBM), the defect band (D band) and the in-plane C sp^2 associated vibration signal (G band) came clearly across in the spectrum at 180–260, 1340, and 1590 cm^{-1}, respectively. In addition, the harmonics and second order vibrations appeared at a higher Raman shift. Moreover, the structural parameter I_D/I_G (or the Raman functionalization marker[38]) for this sample is 0.12, in accordance with a highly preserved nanotube sample. Importantly, the general spectrum shape was maintained for all the functionalized nanotubes, indicating that the tubular scaffold of all samples has been preserved, in accordance with TEM observations (see below). However, the structure was modified according

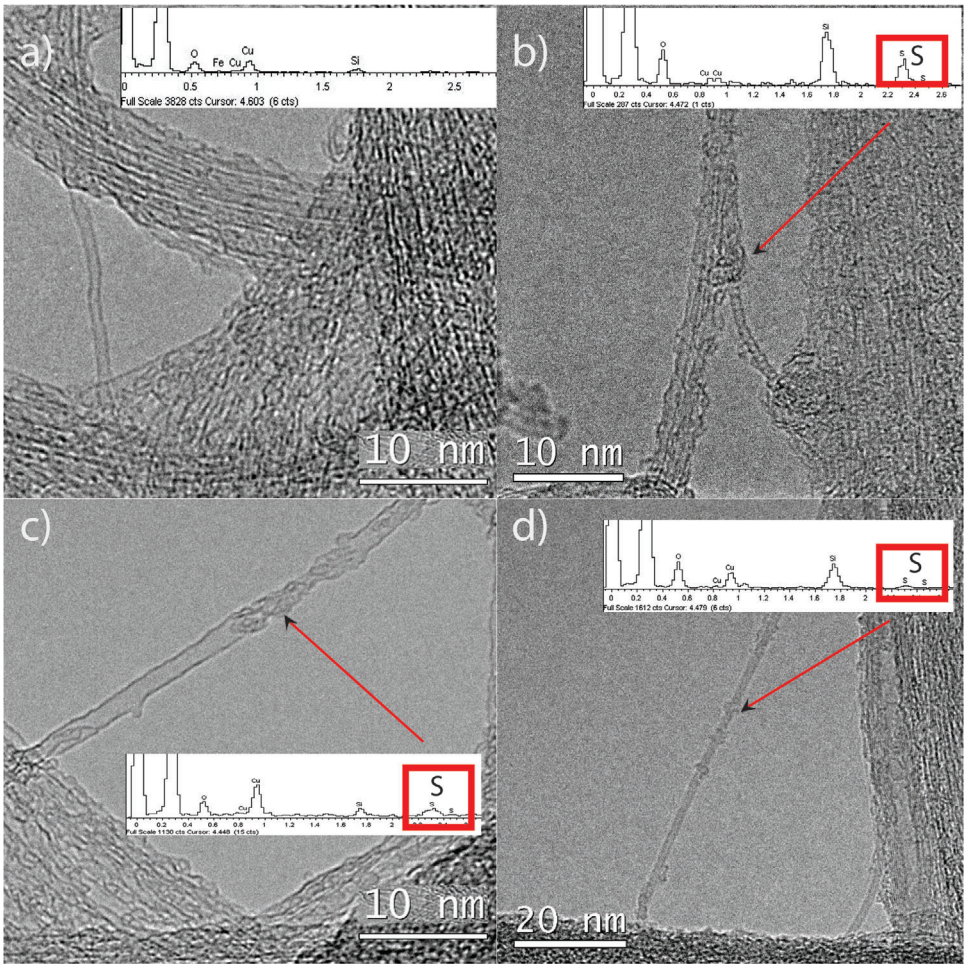

Figure 2. HRTEM images of samples a) **SWNT**, b) **SWNT-PTH-14**, c) **SWNT-PTH-5**, and d) **SWNT-PTH-2**, including the EDX spectrum of each sample (with a zoom of the S signals).

to the functionalization degree. Thus, the structural defectivity decreased as a function of the diminution in bonded PTH since **SWNT-PTH-14** presented an $I_D/I_G = 0.32$, while **SWNT-PTH-5** showed an I_D/I_G ratio of 0.26. Finally, the material with the lowest quantity of PTH, **SWNT-PTH-2**, owned an I_D/I_G ratio of 0.14, which was very close to the purified **SWNT** ($I_D/I_G = 0.12$), corroborating that this sample was functionalized only to a very little extent. Finally, the RBM band, which is sensitive to the diameter of the sample, appeared at the same position in all the SWNT-PTH materials, indicating that the functionalization had taken place at the outer surface of the nanotube.[39] Analyzing the Raman map of the materials, we concluded that a homogeneous functionalization process had occurred. Hence, starting from the optical image, the defective regions, denoted with blue pixels (regions where the D band is maximized), appeared randomly distributed throughout the whole particle while the graphitic regions, that are labeled with red pixels (regions where the G band is maximized) represented the majority of the Raman map. Therefore, the map supposes a reflection of the functionalization. Indeed, from an almost structurally intact particle in the pristine **SWNT** material where red pixels are the major fraction of the mapping, a progressive blue coloration (characteristic of the functionalization) was appearing as the degree of the functionalization was increased (in agreement with the single spectrum measurements), till reaching a more defect-containing particle corresponding to the most functionalized (and defective) sample **SWNT-PTH-14** (**Figure 1**). Comparing the Raman spectra of the functionalized SWNT and pristine **SWNT**, a particular difference was found in the G band. The PTH-functionalized nanotubes showed a G-band with a hypsochromic shift of about 4–7 cm^{-1} compared with the pristine **SWNT** (see Figure S5, Supporting Information). This shift could be indicative of some degree of charge transfer from the PTH catalyst to the nanotube, which is in agreement with the electron-donating character of the PTH unit.[40] This charge transfer effect was also detected by XPS and TAS, as we will discuss below.

The HRTEM images showed in **Figure 2** revealed that the functionalization features discussed above for the SWNT-PTH samples affected the morphology of the nanotubes observed under the microscope. Thereby, the aspect of sample **SWNT-PTH-14**, the most functionalized sample, was rough and the nanotubes appeared clearly covered by the organic catalyst as detected by the in situ EDX analysis performed (for further EDX details, see Figures S6–S9, Supporting Information), which was in stark contrast to the purified nanotubes as introduced above (Figure 2a,b).

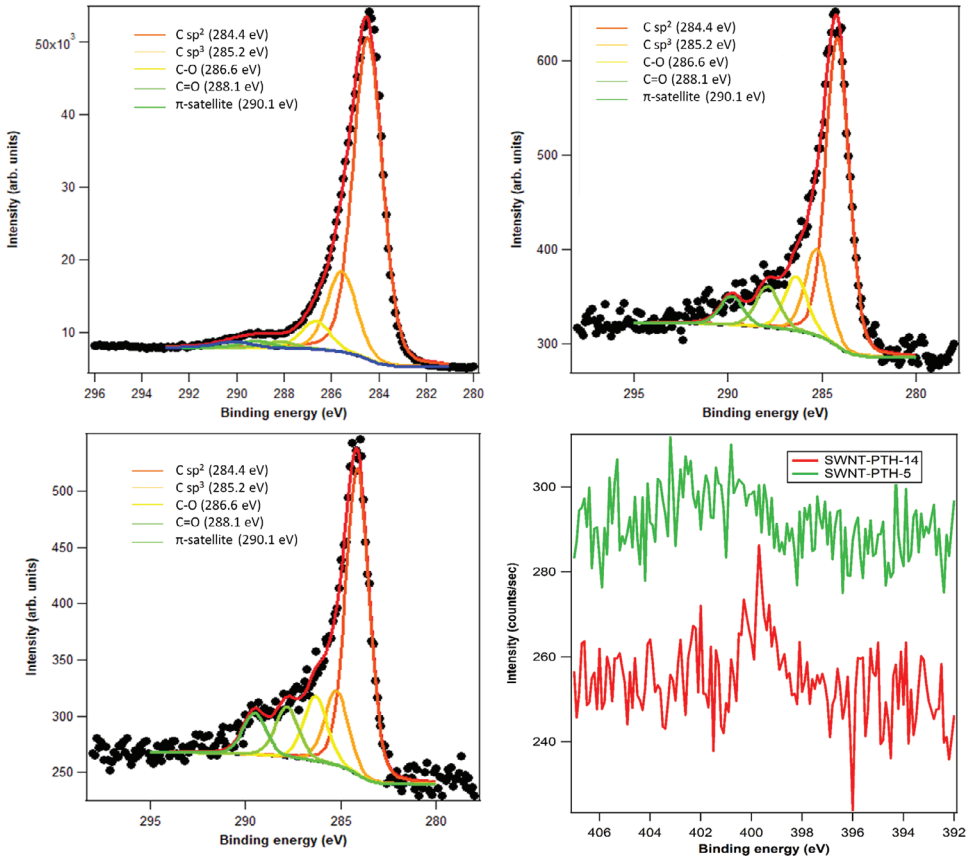

Figure 3. C 1s XPS core level regions of samples a) **SWNT**, b) **SWNT-PTH-14**, and c) **SWNT-PTH-5**. d) N 1s XPS core level region of samples **SWNT-PTH-14** and **SWNT-PTH-5**.

However, in the image of sample **SWNT-PTH-5** the tubular structure of the nanotube could be clearly distinguished from the organic material that populated the surface. In this sample, the tubes appeared smooth and did not show any protrusion or visually distinguishable structural defects, thus indicating that the Raman structural parameter is referred mainly to functionalization events rather than destruction of the carbon nanotube wall integrity.[41] Furthermore, the local analysis of the particle of this sample in the form of EDX mapping (Figure S12, Supporting Information) revealed homogeneous distribution of S signals, which may correspond to a uniform functionalization across the whole nanotube aggregation, in agreement with the previous analysis. Finally, the morphology of sample **SWNT-PTH-2** was very similar to that of the pristine **SWNT**.

The chemical composition of the surface of the samples under study was analyzed by X-ray photoelectron spectroscopy (XPS) (**Figure 3**). The purified sample **SWNT** presented a survey spectrum in which only C 1s (284.5 eV binding energy (BE)) and O 1s (533 eV of BE) core level photoemission peaks could be detected (see Figure S13, Supporting Information). After a fitting procedure, different chemically resolved components in the C 1s spectrum were identified, and the most prominent peak was associated with C sp^2 type bond (284.4 eV of BE, 80%). In addition, a small amount of defective C sp^3 (285.2 eV of BE, 7%) as well as a low content of oxygen related species, including π–π^* transitions (290.1 eV of BE) were found.[42,43] The analysis of the SWNT-PTH functionalized samples revealed the presence of new photoemission signals. Indeed, the survey spectrum of **SWNT-PTH-14** sample showed the presence of N 1s (400 eV of BE) and S 2p (163 eV of BE) photoemission peaks,[44] which are ascribed to the heteroatoms contained in the PTH molecule (Figure 3d; Figure S14, Supporting Information).

These data support the successful covalent functionalization of the nanotube. Nevertheless, these signals associated with heteroatoms were not detected in the sample **SWNT-PTH-2** due to the low functionalization degree of this material, since the amount of heteroatoms is below the detection limit of the technique, according to elemental analysis determinations (see Table 1). As expected, sample **SWNT-PTH-14**, the most defective carbon structure, presented the lowest ratio C sp^2/defects (68%), followed by sample **SWNT-PTH-5** (ratio C sp^2/defects = 76%). This increment in the ratio might indicate that the functionalization has taken place only at the C sp^2 atoms, otherwise the ratio should be constant if any other function had reacted with the functionalizing moiety. Furthermore, solid-state ^{13}C-NMR afforded a single signal in the region C-X (X = O, N, S), which might indicate that the functionalization took place only using the sp^2 wall (see Figure S15, Supporting Information). However, the analysis of the heteroatoms revealed important features (Figure 3 and Supporting Information). While the S 2p core level peak seems to be centered at 163 eV despite the noise, the N 1s peak was surprisingly centered at 401 eV of BE, which can be

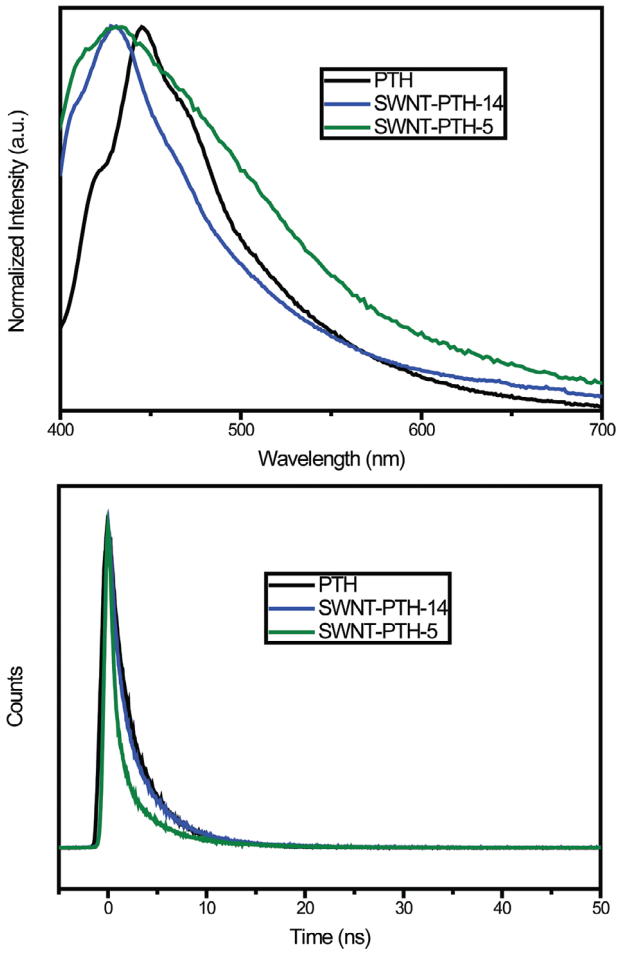

Figure 4. a) Normalized emission spectra of materials **SWNT-PTH-5** and **SWNT-PTH-14** (λ_{ex} = 350 nm) in DMF suspensions, and molecular **PTH** (λ_{ex} = 350 nm) in 10^{-5} M solution in DMF. b) Fluorescence time profiles of **SWNT-PTH-14**, **SWNT-PTH-5**, and **PTH** measured with a 375 nm laser.

indicative of a more electropositive nitrogen.[45,46] This BE shift of the photoemission peak supports the hypothesis of the electron transfer from the nitrogen of the PTH to the SWNT, in agreement with the Raman analysis.

Photoluminescence (PL) experiments of stable suspensions of the materials in DMF were undertaken in addition to time-resolved fluorescence measurements (**Figure 4**). Samples **SWNT-PTH-14** and **SWNT-PTH-5** showed appreciable emission with a band at 448–450 nm, which exhibited a hypsochromic shift of 14–16 nm compared to that of the parent **PTH**. Regarding the emission time profiles, a triexponential fit of the PL decay curve of **PTH** (0.9 ns (16%), 3.0 ns (75%), and 7.8 ns (9%)) was obtained for the DMF solution (**Table 2**). A similar PL decay profile was obtained for DMF suspensions of the materials **SWNT-PTH-14** and **SWNT-PTH-5** (Figure 4b). Thus, the fluorescence lifetimes (τ_F) of **SWNT-PTH-14** were calculated to be 0.9 ns (26%), 3.4 ns (65%), and 9.1 ns (8%). For the **SWNT-PTH-5** sample, the values were recorded as 0.5 ns (42%), 2.6 ns (39%), and 7.3 ns (19%). According to these values, it has been proven that the PTH loading affects the photoluminescence properties of the material. Thus, **SWNT-PTH-5** showed fluorescence lifetimes shorter than those

Table 2. Fluorescence lifetimes (τ_F) of **PTH**, **SWNT-PTH-14**, and **SWNT-PTH-5**; rate constant (k^S_{CS}) and quantum yield of charge separation (Φ^S_{CS}) of **SWNT-PTH-5**.

Sample	τ_F, [ns (%)]	k^S_{CS} [s^{-1}]	Φ^S_{CS}
PTH	0.9 (16)		
	3.0 (75)		
	7.8 (9)		
SWNT-PTH-14	0.9 (26)		
	3.4 (35)		
	9.1 (8)		
SWNT-PTH-5	0.5 (42)	$8.9 \cdot 10^{+8}$	0.44
	2.6 (39)	$5.1 \cdot 10^{+7}$	0.13
	7.3 (19)	$1.4 \cdot 10^{+8}$	1

$k^S_{CS} = 1/\tau_{F(material)} - 1/\tau_{F(PTH)}$; $\Phi^S_{CS} = k^S_{CS} \cdot \tau_{F(material)}$.

of molecular **PTH**, suggesting an effective deactivation of PTH* in the nanotube. Moreover, for the sample **SWNT-PTH-5**, the charge separation rate constants (k^S_{CS}) and quantum yield of the charge separation (Φ^S_{CS}) of the three τ_F components were calculated (Table 2). These values suggested that an efficient charge separation had occurred within **SWNT-PTH-5**, which would also explain the photocatalytic performance showed by this material (see below).

In an attempt to shed light on the photophysical phenomena, Transient Absorption Spectroscopy (TAS) experiments were carried out. We thought that the **PTH** triplet state could in principle be a reactive excited state. Excitation of **PTH** molecule at 355 nm resulted in an intense peak at 460 nm, which was assigned to the characteristic triplet-triplet absorption of **PTH** (**Figure 5**A, black line).[47]

To identify a possible triplet quenching, this experiment was also performed upon addition of **SWNT** powder, which was suspended in the organic phase by sonication. Interestingly, a diminished absorption at 460 nm was observed (Figure 5A, red line). Indeed, a marked decrease of the **PTH** lifetime resulted in the presence of **SWNT**, suggesting the involvement of the **PTH** triplet in an electron transfer process (Figure 5B).

Similar TAS studies were conducted for **SWNT-PTH-5** hybrid material working at the same laser power excitation with optically matched disperse solutions at 355 nm. The relative population of charge separated states at the same laser time can be drawn by comparing the intensity of the transient signals. **Figure 6**A shows the transient spectra recorded for **SWNT-PTH-5** at 0.25, 2, 40, and 60 μs after the laser pulse. First, the signal recorded for **SWNT-PTH-5** was about seven times weaker than that monitored for **PTH**. In addition, the transient spectrum for **SWNT-PTH-5** is a continuous absorption in the complete spectral range, dominated by a very broad absorption from 450 to 800 nm. This continuous absorption is not uncommon for transient spectra in carbon nanotubes and derivatives and has been attributed to electrons and holes localized on the carbonaceous wall.[48–50] Decay trace at 460 nm were found to fit well with two-order kinetics,

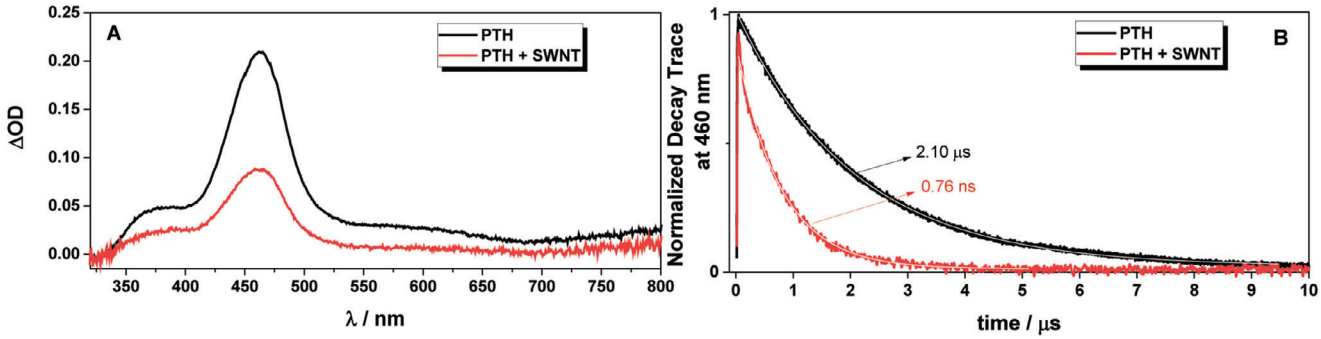

Figure 5. A) Transient absorption spectra (λ_{exc} = 355 nm; ≈20 mJ pulse^{-1}) of **PTH** (0.15 mM) in DMF solution (black) and **PTH** (0.15 mM) in the presence of **SWNT** in DMF dispersion solution (red). Both spectra were recorded at 0.5 μs after laser excitation. B) Decay kinetics (λ_{exc} = 355 nm; ≈20 mJ pulse^{-1}) at 460 nm of **PTH** (0.15 mM) in DMF solution (black) and PTH (0.15 mM) in the presence of **SWNT** in DMF dispersion solution (red). The white lines indicate the goodness of the lifetime measurement fitting.

distributed in two major populations for the charge separated transient state (Figure 6B, black): charge carriers closely localized where photochemical event occurs (shortest lifetimes) and further migration and delocalization in the particle (longest lifetime fraction). Lifetime values were in well agreement with previously reported data (ns time scale),[51] with a major contribution for the shorter lifetime component. Temporal profiles at 460 nm in the μs scale were also recorded for both **SWNT-PTH-5** and **SWNT-PTH-14** (Figure 6B, inset). Interestingly, decay traces exhibited a first faster component shorter than 1 μs (vide supra), then a growth took place in the first 3 μs together with a subsequent slower decay. We believe that this result could be interpreted as a fast charge recombination (prompt decay), migration of the charge through the material surface (growth of the signal) and non-coupled recombination after random work. Clearly, this enhancement of the signal for **SWNT-PTH-5** in comparison with the **SWNT-PTH-14** features suggested that production of charge separation was remarkably higher in **SWNT-PTH-5**, which may justify the catalytic activity observed (see below).

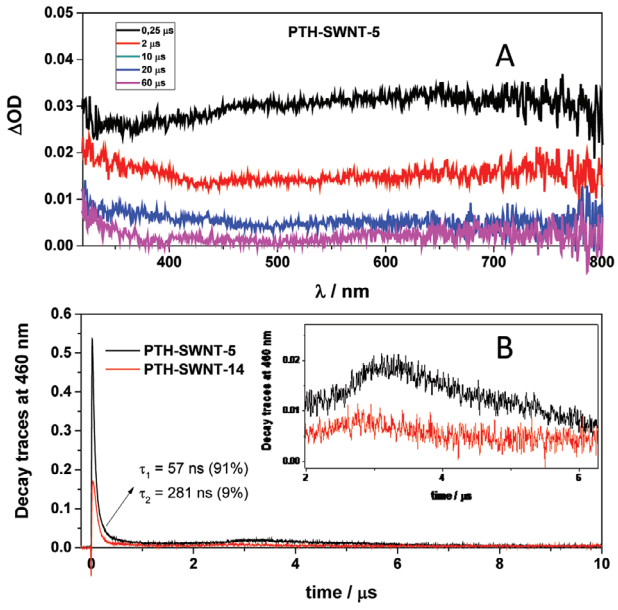

Figure 6. A) Transient absorption spectra (λ_{exc} = 355 nm; ≈20 mJ pulse^{-1}) of **SWNT-PTH-5** in DMF dispersion solution. B) Temporal profiles (λ_{exc} = 355 nm; ≈20 mJ pulse^{-1}) of the transient signal monitored at 460 nm for **SWNT-PTH-5** (black) and **SWNT-PTH-14** (red) in DMF dispersion solution.

2.2. Catalytic Activity

The photocatalytic activity of the materials was evaluated and compared to that of the parent **PTH**. The PTH organophotocatalyst and its derivatives are well established for a wide gamut of dehalogenation reactions[7] due to its high reduction potential that can trigger the reduction of the C—Br bond [$E°$ (PTH$^{•+}$/PTH*) = −2.1 V versus SCE; $E°$ (PTH$^{•+}$/PTH) = 0.68 V versus SCE].[6] For this reason we have chosen, as the model reaction, the photoreduction of *p*-bromobenzonitrile **1a**, in the presence of Bu_3N and HCOOH, under inert atmosphere in acetonitrile using 420 nm light irradiation (**Table 3**). With just 1 mg of the hybrid material **SWNT-PTH-X** (**X = 2–14**) as catalyst, we detected some reactivity differences as a function of the material employed during a typical 16 h run. Indeed, only catalysts **SWNT-PTH-14** and **SWNT-PTH-5** showed catalytic activity (Table 3 entries 1–2). In particular, **SWNT-PTH-14** achieved an 88% conversion of the reduced product **2a**, whereas **SWNT-PTH-5** was able to fully reduce the substrate **1a**. Conversely, the material with the lowest PTH-content, **SWNT-PTH-2**, presented negligible activity, as did the non-functionalized **SWNT** (Table 3 entries 3–4). Finally, the control tests performed without either the catalyst, the base, the acid or the light showed the importance of those components in triggering the photochemical reactivity (Table 3, entries 5–8). Therefore, all the experiments performed with the hybrid materials indicate that the loading of covalently bonded PTH at the nanotube surface is a key factor in their catalytic performance, with 5% PTH being the optimal loading at the SWNT surface. This evidence agrees with the efficient charge separation detected in the fluorescence decay of material **SWNT-PTH-5** (see Table 2 and Figure 4b). This effect was not observed when this reaction was performed with the molecular catalyst under homogeneous conditions. A typical 5 mol.% loading of **PTH** resulted in an 80% conversion after 16 h light irradiation (Table 3 entry 9).[7] Nonetheless, decreasing the loading to 0.1 mol.% versus substrate **1a**

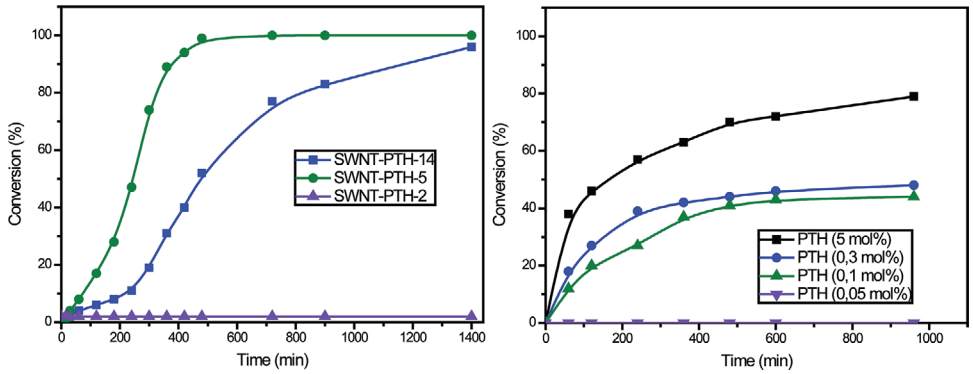

Figure 7. Temporal evolution tracked by ^{1}H-NMR spectroscopy of the photo-debromination of **1a** catalyzed by a) heterogeneous nanotube-based catalysts **SWNT-PTH-X** and b) homogeneous **PTH** at different loadings.

(comparable PTH loading as **SWNT-PTH-5**) presented only a 43% conversion in the reduction of **1a** (Table 3 entry 10). These results highlight the outperformance of the hybrid material compared with the homogeneous catalyst under the same conditions. In addition, the activity has been compared with other state-of-the-art catalysts for similar transformations (see Table S3, Supporting Information), finding that this covalently functionalized material performs at the same level or better than other photoactive nanocarbons, quantum dots, TiO_2 and related systems (even including those doped with noble metals) and very active covalent organic frameworks.

Motivated by the intriguing catalytic behavior of our hybrid materials, we wanted to gain insights into the activity by monitoring the progress of the debromination reaction of **1a** by ^{1}H-NMR technique using the different hybrid materials as catalysts (**SWNT-PTH-X**) as well as the homogeneous **PTH** catalyst. The results of these experiments are shown in **Figure 7**. As previously commented in Table 3, the material **SWNT-PTH-2**, which contained the lowest PTH loading, showed negligible activity in a monitored 24 h reduction run (Figure 7a). Such lack of activity was also observed under homogeneous **PTH** amounts as low as 0.05 mol.% (Figure 7b). On the other hand, the catalysts **SWNT-PTH-14** and **SWNT-PTH-5** were active for the debromination of substrate **1a**, showing that **SWNT-PTH-5** had the best catalytic performance. This material presented a sigmoidal kinetic profile similar to other heterogeneous SWNT-based catalysts reported previously,[34,35] achieving a conversion above 90% in 5 h, and a full conversion in just 7 h. Indeed, **SWNT-PTH-5** was even able to surpass the best result conducted under homogenous **PTH** (5 mol.%). Nevertheless, the differences in the catalytic performance of **SWNT-PTH-14** and **SWNT-PTH-5** cannot solely be explained based on the PTH content, as the material with the lowest content of functionalized organophotocatalyst was the most active. According to the Raman and XPS data discussed above, **SWNT-PTH-14** presents a higher defect concentration than **SWNT-PTH-5**. Therefore, the electronic communication between the PTH motif and the nanotube structure, the electron conduction across and the charge separation in **SWNT-PTH-14** catalyst might be less efficient. This explanation agrees with the longer fluorescence decay exerted by **SWNT-PTH-14** compared with **SWNT-PTH-5** and the TAS data.

On another hand, the homogeneous catalyst **PTH** (Figure 7b) displayed an expected higher debromination conversion of substrate **1a** as the amount of catalyst increases in the reaction. Thus, after a reaction time of 1 h a 12% conversion was achieved when 0.3 mol.% of **PTH** was added as the catalyst. The conversion value increased up to 38% by adding 5 mol.% of organophotocatalyst. However, the catalytic performance of homogeneous **PTH** was always inferior to the PTH bounded to SWNT. In summary, these experiments showed the importance of controlling the photocatalyst loading into SWNT to obtain a good electronic communication between the photoactive molecule and the SWNT core, as well as a good efficient charge separation, both key factors for an optimal photocatalytic performance.

According to these observations, the mechanism proposed to explain the photocatalytic activity of **SWNT-PTH-5** is outlined in **Scheme 3**. Under light irradiation, the small amount of PTH motifs decorating the outer surface of the nanotube is able to

Table 3. Model debromination reaction photocatalyzed by the materials.

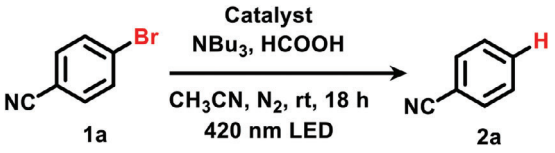

Entry[a)]	Variation	Conversion [%][b)]
1	Catalyst = **SWNT-PTH-14**	88
2	Catalyst = **SWNT-PTH-5**	>99
3	Catalyst = **SWNT-PTH-2**	n.r.
4	Catalyst = **SWNT**	n.r.
5	No catalyst	18
6	No base	n.r
7	No acid	32
8	No light	n.r.
9	Catalyst = **PTH** (5 mol%)	80
10	Catalyst = **PTH** (0.1 mol%)	43

[a)] Reaction conditions: substrate **1a** (0.1 mmol), Bu_3N (5 equiv.), HCOOH (5 equiv.) and 1 mg of heterogeneous catalyst in acetonitrile (1 mL) under an inert atmosphere were irradiated under 420 nm light for 16 h at rt. The homogeneous **PTH** loading is expressed in mol%; [b)] Conversion (%) determined by ^{1}H-NMR; n.r. stands for no reaction.

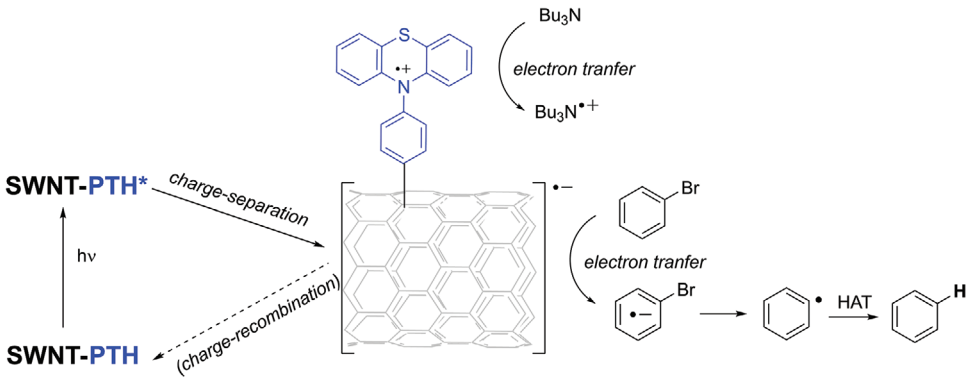

Scheme 3. Mechanistic proposal for the reduction of aryl-halides.

inject electrons into the nanotube π system, producing electron-holes pairs spatially separated, which suppress the recombination of the photogenerated excitons. Then, a single electron transfer from the photogenerated electrons at the SWNT surface to the arylbromide **1a** occurs, facilitating the cleavage of the C-Br bond and subsequently the formation of the aryl radical. To recover the initial catalytic material, tributylamine acts as a sacrificial electron donor, transferring an electron to the PTH moiety. Finally, the radical follows a hydrogen atom transfer process (HAT) to give the final product.

With the best catalyst in hand, we studied the durability and recyclability of the hybrid material **SWNT-PTH-5**. Indeed, a very important parameter for any heterogeneous catalyst is its ability to be recycled and maintain its catalytic activity.[52] To accomplish this task, catalyst **SWNT-PTH-5** was recovered by filtration using a PTFE membrane, and then washed profusely with organic solvents to remove any adsorbed species. Once recovered and clean, the nanotube-based powder was used for a new catalytic cycle without adding, in any case, fresh catalyst. This recycling sequence was performed for 5 consecutive runs in the photodebromination of **1a** catalyzed by **SWNT-PTH-5** under standard conditions (**Figure** 8a). Remarkably, the nanotube-based photocatalyst was able to maintain its catalytic activity throughout all the recycling study, with a constant level of conversion above 98% in the five recovery experiments. Conversely, a homogeneous endurance test with catalyst **PTH** did not show any activity beyond the first cycle (Figure 8a), highlighting the stability and protection effect of the material into the photocatalyst by covalent functionalization. In addition, leaching experiments were performed for the catalysts **SWNT-PTH-14** and **SWNT-PTH-5**. These experiments were performed adopting a "hot filtration" configuration,[34] filtering out the catalyst and allowing the reaction to proceed further for some additional time. The filtration was performed at ≈50% conversion level. After the removal of the catalyst (Figure 8b), the hydrodebromination of **1a** was stopped for both catalysts, **SWNT-PTH-14** and **SWNT-PTH-5**, indicating that there were not any soluble species in the reaction medium responsible for the catalytic activity observed. Finally, the characterization of the recovered catalyst **SWNT-PTH-5** by Raman spectroscopy and SEM/TEM microscopies (including in situ EDX analysis) presented a nanotube-based material with an I_D/I_G ratio of 0.27 of individual and clean nanotubes very similar

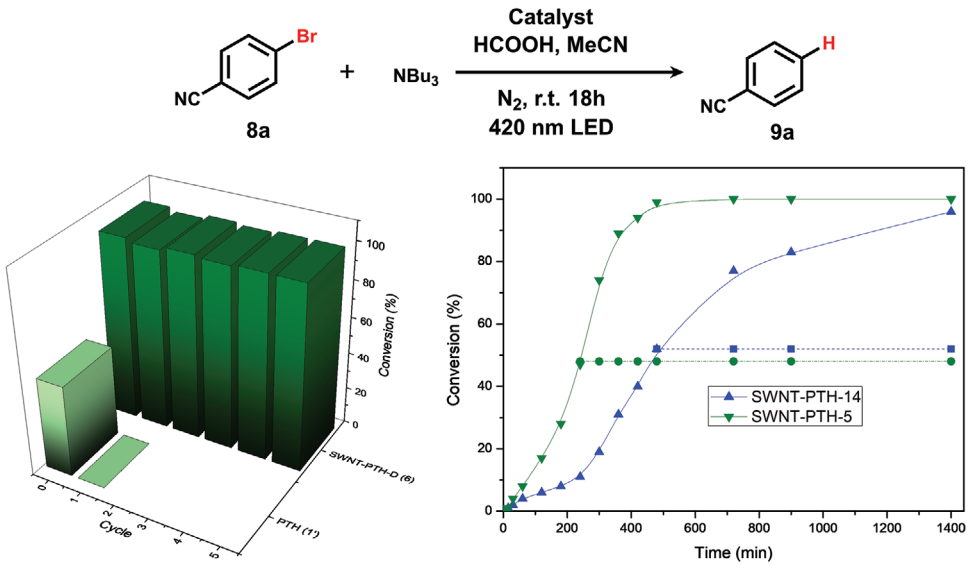

Figure 8. Catalytic performance study by: a) a recycling study and b) a hot filtration experiment for leaching elucidation.

Table 4. Debromination of different substrates **1** catalyzed by **SWNT-PTH-5**.[a)]

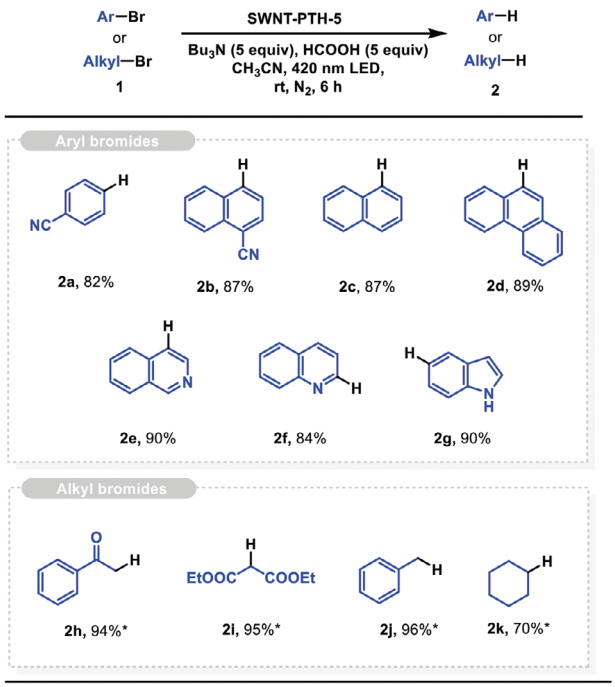

[a)] Reaction Conditions: substrate 1 (0.1 mmol), Bu_3N (5 equiv), HCOOH (5 equiv) and 1 mg of **SWNT-PTH-5** in acetonitrile (1 mL) under an inert atmosphere were irradiated under 420 nm light for 6 h at rt. Values stand for isolated yield; *Denotes ^{1}H-NMR yield determined using CH_3NO_2 as internal standard.

to the fresh sample as it can be seen in the microscopy images (see Figures S16–S18, Supporting Information), with elemental analysis values very close to the non-reacted sample, thus indicating that no chemical or morphological modification of the hybrid material occurred after the catalytic run.

To evaluate the versatility of catalyst **SWNT-PTH-5**, we studied the debromination reaction of a variety of substrates **1** (**Table 4**). Moreover, we took advantage of the affinity of the carbon nanomaterial for the polyaromatic substrates to improve the debromination performance using a synergistic effect based on substrate preconcentration at the surface by π–π interactions.[34,53,54] However, homogeneous photocatalysts usually struggle to successfully debrominate those polyaromatic substrates. Indeed, substrate *p*-bromobenzonitrile **1a**, which only contained one aromatic ring, was debrominated with a very good yield (82%). Conversely, the larger aromatic surface of the 4-bromo-1-naphthonitrile **1b** gave a better yield (87%) due to a better π-stacking compared with the phenyl ring. The same results were obtained using 1-bromonaphthalene **1c**, and 1-bromophenanthrene **1d**, which were debrominated with yields of 87% and 89%, respectively.

N-containing polyheterocycles were also well debrominated, affording isoquinoline **2e** (90% yield), quinoline **2f** (84% yield) and indole **2 g** (90% yield). In addition, alkyl-bromides such as bromoacetophenone **1 h** and diethyl bromomalonate **1i** were also photodebrominated using **SWNT-PTH-5** with yields of 94% and

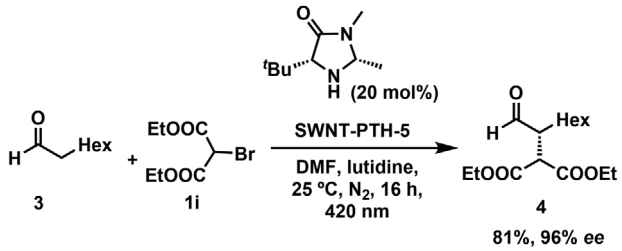

Scheme 4. Enantioselective α-alkylation of aldehydes catalyzed by **SWNT-PTH-5** and MacMillan's imidazolidinone.

95% respectively. Moreover, aliphatic substrates, such as benzyl bromide **1j** or cyclohexyl bromide **1k** could be straightforwardly reduced by the modified nanotube catalyst in yields of 94% and 70%, respectively. Finally, the synthetic utility of the covalently functionalized nanotube photocatalyst was examined in the α-alkylation of aldehydes with bromo diethylmalonate (**1i**), which is an organic transformation that combines two different catalytic cycles: one photocatalytic debromination and an enantioselective alkylation mediated by an organocatalyst (**Scheme 4**).[55,56] More specifically, the explored reaction consisted of the alkylation of octanal (**3**) with the malonate radical derived from **1i** under MacMillan's imidazolidinone and **SWNT-PTH-5** catalysts. Under these conditions, the corresponding alkylated product **4** was successfully obtained with a very good yield (81%) with a 96% of enantiomeric excess.

3. Conclusion

This work describes the direct covalent functionalization of SWNT with a known organic photocatalyst, 10-phenylphenothiazine **PTH**, through diazonium chemistry. As a result, a direct covalent bond between both units was formed, as demonstrated by several characterization techniques. We employed different amounts of **PTH** in the functionalization, achieving hybrid materials with an increasing organophotocatalyst loading, **SWNT-PTH-X (X = 2, 5, 14)**. Interestingly, the structure and photochemical properties of the hybrids obtained was found to be different as a consequence of the amount of PTH introduced. Indeed, the most efficient charge separation and charge transfer between the nanotube and the photoactive motif was observed for sample **SWNT-PTH-5**, which was functionalized with a 5% PTH loading. Conversely, the most functionalized sample **SWNT-PTH-14** presented a poorer photoactive activity as a consequence of a more defective structure according to elemental analysis, TGA, Raman and XPS data, while **SWNT-PTH-2** was not photoactive at all due to its low functionalization, elucidated by solid characterization techniques too. Therefore, the photocatalytic performance in the dehalogenation reaction of aromatic bromides matched this range of properties. The most active catalyst was sample **SWNT-PTH-5**, which was able to complete the reaction in <7 h, outperforming the other nanotube samples and the homogeneous tests, presenting a broad scope and being compatible with other catalysts for performing dual catalysis, such as estereoselective α-alkylations. In addition, the sample **SWNT-PTH-5** presented a fully recyclable performance without observing any leaching due to the covalent bond. We believe that this

work paves the way toward managing direct bonding between carbon nanotubes and photoactive motifs for photocatalytic purposes.

4. Experimental Section

Materials and Methods: All chemicals, solvents, and reagents, including single-walled carbon nanotubes (SWNT, Aldrich), were purchased from commercial sources (reagent grade quality or better) and used without further purification if not otherwise stated. The purification of organic products, when necessary, was accomplished by flash chromatography using silica gel (Merck Geduran Si 60) in an adequate mixture of cyclohexane (CyH) and ethyl acetate (EtOAc) eluents. All the organic products were characterized by a comparison of their ^{1}H NMR spectral data with those reported in the literature or from commercial sources. The synthesis of compounds **PTH**[31] and **PTH-NH$_2$**[32] are fully described in the Supporting Information. Characterization methods are fully reported in the Supporting Information too.

Nanotube Functionalization: *Synthesis of SWNT-PTH-X*: First, commercially available SWNT (50 mg) were treated with concentrated hydrochloric acid, and the mixture was magnetically stirred at 60 °C for 2 h. After cooling down, the solid was isolated by centrifugation and washed with fresh Milli-Q water with the necessary centrifugation cycles until the supernatant reached neutral pH. After drying under vacuum, the procedure yielded the purified **SWNT** sample.[24,25] A sample of 12 mg of **SWNT** was placed in a round bottom flask with the corresponding amount of **PTH-NH$_2$**. To this mixture, 20 mL of *N*-methylpyrrolidinone (NMP) and the corresponding amount of isoamyl nitrite were added sequentially. The reaction was magnetically stirred at 80 °C for 1 h. Then, the reaction mixture was allowed to naturally cool to room temperature, and the suspension was filtered through a 0.45 µm polytetrafluoroethylene (PTFE) membrane. The black powder was collected, suspended in 20 mL of *N.N*-dimethylformamide (DMF), sonicated for 1 min, and filtered again. This washing procedure was repeated with DMF (4 × 20 mL), methanol (3 × 20 mL), water (2 × 20 mL), methanol (2 × 20 mL), and finally with acetone (2 × 20 mL). Drying under vacuum produced the corresponding **SWNT-PTH-X** sample. For **SWNT-PTH-14**, 87 mg (0.3 mmol) of **PTH-NH$_2$** and 81 µL (0.6 mmol) of isoamyl nitrite were added. For **SWNT-PTH-5**, 8.7 mg (0.03 mmol) of **PTH-NH$_2$** and 8.1 µL (0.06 mmol) of isoamyl nitrite were added. For **SWNT-PTH-2**, 0.87 mg (0.003 mmol) of **PTH-NH$_2$** and 0.8 µL (0.006 mmol) of isoamyl nitrite were added.

Catalysis—General Photocatalytic Debromination: A vial was charged with a magnetic stirring bar, the corresponding halogenated substrate **1** (0.1 mmol), the catalyst (1 mg for nanotube-based materials, 0.05–5 mol % for **PTH**), CH_3CN (1 mL), HCOOH (0.5 mmol), and Bu_3N (0.5 mmol). The vial was sealed and degassed by 3 N_2-freeze-pump-thaw cycles. The reaction was irradiated under blue LED (420 nm) and stirred for the appropriate time, typically 6 h. A 0.05–0.1 mL aliquot was withdrawn at regular intervals and analyzed by ^{1}H-NMR spectroscopy to monitor the progress of the reaction. The yields of volatile products were calculated by ^{1}H-NMR using CH_3NO_2 as the internal standard whereas the non-volatile compounds were purified by flash chromatography to calculate the isolated yield. The full experimental details for each product **2** and **4,** and their characterization data, are described in the Supporting Information.

General Procedure for the α-alkylation of Aldehydes: A vial containing diethyl bromomalonate (**1i**) (0.1 mmol), octanaldehyde (**3**) (0.2 mmol), 2,6-lutidine (0.36 mmol), DMF (0.5 mL), (*R,R*)−2-*tert*-butyl-3,5-dimethylimidazolidin-4-one (10 mg, 0.04 mmol), and 1 mg of catalyst **SWNT-PTH-5** was charged with a magnetic stirring bar. The vial was sealed and degassed by three freeze-pump-thaw cycles. The reaction was irradiated under blue LED (420 nm) and stirred for 16 h. The nanotubes were then filtrated over a PTFE membrane, and the filtrate was diluted with EtOAc and washed with a 10% aqueous solution of LiCl (3x) and water (2x). The organic layer was dried over $MgSO_4$ and concentrated under vacuum. The crude material was subjected to a Wittig reaction with benzyl (triphenylphosphoranylidene) acetate (2 equivalents) in dichloromethane (0.1 M) for 4 h. The reaction mixture was then concentrated, and the product purified by flash chromatography. The enantiomeric excess was determined by supercritical fluid chromatography (SFC).[33]

Recycling and Leaching Experiments: After the reaction was completed, the nanotube-based photocatalysts were recovered by filtration through polytetrafluoroethylene (PTFE) membranes, and then washed three times with acetone and three further times with dichloromethane, sonicating for 5 min between each cycle, and the solid was finally vacuum-dried. Following this procedure, the heterogeneous catalyst was employed in a new catalytic cycle by adding all the reagents and solvents. This procedure was repeated several times. In the case of the homogeneous photocatalyst, the recyclability was assessed performing endurance tests. To perform this task, the typical debromination of substrate **1a** was set using 0.1 mol.% loading of PTH, and the conversion of this reaction was monitored by ^{1}H-NMR after 16 h of illumination. Then, a fresh reactant mixture was added to the reaction vessel, and it was allowed to proceed again under inert atmosphere for additional 16 h of illumination to furtherly monitor the outcome of this reactant addition. For the leaching experiments, a typical hot-filtration configuration was adopted.[34] To perform this task, the debromination of **1a** using catalyst **SWNT-PTH-5** or **SWNT-PTH-14** was allowed to proceed to reach ≈50% conversion (500 min for **SWNT-PTH-14** and 250 min for **SWNT-PTH-5**). The reaction was stopped, the heterogeneous catalyst was filtrated off, and the system was set again under inert atmosphere and returned to the LED. The filtrate mixture was monitored by withdrawing aliquots at regular intervals and analyzing them by ^{1}H-NMR spectroscopy.

Supporting Information

Supporting Information is available from the Wiley Online Library or from the author.

Acknowledgements

This work was supported by the MICINN (PID2021-122299NB-100, TED2021-129999B-C32, and TED2021-130470B-100), VIRMAT Projects in response to COVID-19 financed by the ERDF-REACT-EU resources, "Comunidad de Madrid" for European Structural Funds (S2018/NMT-4367) and proyectos sinérgicos I+D (Y2020/NMT-6469). J.L.N.-F. thanks "Comunidad de Madrid" for the industrial doctorate fellowship (IND2019/AMB-17142).

Conflict of Interest

The authors declare no conflict of interest.

Data Availability Statement

The data that support the findings of this study are available from the corresponding author upon reasonable request.

Keywords

carbon nanotubes, covalent functionalization, electronic communication, phenothiazines, photocatalysis

Received: October 23, 2023
Revised: November 30, 2023
Published online:

[1] C. K. Prier, D. A. Rankic, D. W. C. Macmillan, *Chem. Rev.* **2013**, *113*, 5322.
[2] N. A. Romero, D. A. Nicewicz, *Chem. Rev.* **2016**, *116*, 10075.
[3] J. M. R. Narayanam, C. R. J. Stephenson, *Chem. Soc. Rev.* **2011**, *40*, 102.
[4] F. Glaser, O. S. Wenger, *Coord. Chem. Rev.* **2020**, *405*, 213129.
[5] S. G. E. Amos, M. Garreau, L. Buzzetti, J. Waser, *Beilstein J. Org. Chem.* **2020**, *16*, 1163.
[6] X. Pan, C. Fang, M. Fantin, N. Malhotra, W. Y. So, L. A. Peteanu, A. A. Isse, A. Gennaro, P. Liu, K. Matyjaszewski, *J. Am. Chem. Soc.* **2016**, *138*, 2411.
[7] E. H. Discekici, N. J. Treat, S. O. Poelma, K. M. Mattson, Z. M. Hudson, Y. Luo, C. J. Hawker, J. R. De Alaniz, *Chem. Commun.* **2015**, *51*, 11705.
[8] Y. Kwon, J. Lee, Y. Noh, D. Kim, Y. Lee, C. Yu, J. C. Roldao, S. Feng, J. Gierschner, R. Wannemacher, M. S. Kwon, *Nat. Commun.* **2023**, *14*, 92.
[9] F. Wang, C. Wang, Z. Yu, Q. He, X. Li, C. Shang, Y. Zhao, *RSC Adv.* **2015**, *5*, 70086.
[10] K. Woan, G. Pyrgiotakis, W. Sigmund, *Adv. Mater.* **2009**, *21*, 2233.
[11] V. Popov, *Mater. Sci. Eng. R* **2004**, *43*, 61.
[12] Y. Yan, J. Miao, Z. Yang, F.-X. Xiao, H. B. Yang, B. Liu, Y. Yang, *Chem. Soc. Rev.* **2015**, *44*, 3295.
[13] S. S. D. Atula, T. Yutaka, U. Tetsuya, S. Yuuki, M. Yu, A. Yasuyuki, I. Osamu, *Chem. Lett.* **2006**, *35*, 1188.
[14] X.-Y. Xie, J.-J. Yang, X.-Y. Liu, Q. Fang, W.-H. Fang, G. Cui, *Phys. Chem. Chem. Phys.* **2021**, *23*, 13503.
[15] M. A. Fox, M. T. Dulay, *Chem. Rev.* **1993**, *93*, 341.
[16] B. Dai, J. Fang, Y. Yu, M. Sun, H. Huang, C. Lu, J. Kou, Y. Zhao, Z. Xu, *Adv. Mater.* **2020**, *32*, 1906361.
[17] Y. Wan, Q. Liang, T. Cong, X. Wang, Y. Tao, M. Sun, Z. Li, S. Xu, *RSC Adv.* **2015**, *5*, 66286.
[18] R. Chitta, A. S. D. Sandanayaka, A. L. Schumacher, L. D'Souza, Y. Araki, O. Ito, F. D'Souza, *J. Phys. Chem. C* **2007**, *111*, 6947.
[19] Z. Yang, H. Pu, J. Yuan, D. Wan, Y. Liu, *Chem. Phys. Lett.* **2008**, *465*, 73.
[20] K.-Q. Lu, Y.-H. Li, Z.-R. Tang, Y.-J. Xu, *ACS Mater. Au* **2021**, *1*, 37.
[21] G. Bottari, G. De La Torre, D. M. Guldi, T. Torres, *Chem. Rev.* **2010**, *110*, 6768.
[22] J. L. Bahr, J. Yang, D. V. Kosynkin, M. J. Bronikowski, R. E. Smalley, J. M. Tour, *J. Am. Chem. Soc.* **2001**, *123*, 6536.
[23] N. Tagmatarchis, M. Prato, *J. Mater. Chem.* **2004**, *14*, 437.
[24] M. Blanco, S. Cembellín, S. Agnoli, J. Alemán, *ChemCatChem* **2021**, *13*, 5156.
[25] N. Mackiewicz, J. A. Delaire, A. W. Rutherford, E. Doris, C. Mioskowski, *Chem. - Eur. J.* **2009**, *15*, 3882.
[26] S. Settele, F. J. Berger, S. Lindenthal, S. Zhao, A. A. El Yumin, N. F. Zorn, A. Asyuda, M. Zharnikov, A. Högele, J. Zaumseil, *Nat. Commun.* **2021**, *12*, 2119.
[27] J. A. Robinson, E. S. Snow, S. C. Badescu, T. L. Reinecke, F. K. Perkins, *Nano Lett.* **2006**, *6*, 1747.
[28] S. Banerjee, T. Hemraj-Benny, S. ? S. Wong, *Adv. Mater.* **2005**, *17*, 17.
[29] T. Arai, S. Nobukuni, A. S. D. Sandanayaka, O. Ito, *J. Phys. Chem. C* **2009**, *113*, 14493.
[30] R. Martín, L. B. Jiménez, M. Álvaro, J. C. Scaiano, H. García, *Chem. - Eur. J.* **2009**, *15*, 8751.
[31] D. González-Muñoz, A. Gómez-Avilés, C. B. Molina, J. Bedia, C. Belver, J. Alemán, S. Cabrera, *J. Mater. Sci. Technol.* **2022**, *103*, 134.
[32] L. Mayer, L. May, T. J. J. Müller, *Org. Chem. Front.* **2020**, *7*, 1206.
[33] A. Casado-Sánchez, M. Uygur, D. González-Muñoz, F. Aguilar-Galindo, J. L. Nova-Fernández, J. Arranz-Plaza, S. Díaz-Tendero, S. Cabrera, O. García Mancheño, J. Alemán, *J. Org. Chem.* **2019**, *84*, 6437.
[34] D. González-Muñoz, J. Alemán, M. Blanco, S. Cabrera, *J. Catal.* **2022**, *413*, 274.
[35] M. A. Valle-Amores, M. Blanco, S. Agnoli, A. Fraile, J. Alemán, *J. Catal.* **2022**, *406*, 174.
[36] H.-J. Yen, G.-S. Liou, *J. Mater. Chem. A* **2010**, *20*, 9886.
[37] L. Fernández-García, M. Blanco, C. Blanco, P. Álvarez, M. Granda, R. Santamaría, R. Menéndez, *J. Mol. Catal. A* **2016**, *416*, 140.
[38] M. S. Dresselhaus, A. Jorio, M. Hofmann, G. Dresselhaus, R. Saito, *Nano Lett.* **2010**, *10*, 751.
[39] B. Nieto-Ortega, J. Villalva, M. Vera-Hidalgo, L. Ruiz-González, E. Burzurí, E. M. Pérez, *Angew. Chem., Int. Ed.* **2017**, *56*, 12240.
[40] A. M. Rao, P. C. Eklund, S. Bandow, A. Thess, R. E. Smalley, *Nature* **1997**, *388*, 257.
[41] J.-Y. Mevellec, C. Bergeret, J. Cousseau, J.-P. Buisson, C. P. Ewels, S. Lefrant, *J. Am. Chem. Soc.* **2011**, *133*, 16938.
[42] M. Favaro, S. Agnoli, C. Di Valentin, C. Mattevi, M. Cattelan, L. Artiglia, E. Magnano, F. Bondino, S. Nappini, G. Granozzi, *Carbon* **2014**, *68*, 319.
[43] M. Blanco, D. Mosconi, M. Otyepka, M. Medved, A. Bakandritsos, S. Agnoli, G. Granozzi, *Chem. Sci.* **2019**, *10*, 9438.
[44] M. Blanco, M. Lunardon, M. Bortoli, D. Mosconi, L. Girardi, L. Orian, S. Agnoli, G. Granozzi, *J. Mater. Chem. A.* **2020**, *8*, 11019.
[45] R. K. Blundell, P. Licence, *Phys. Chem. Chem. Phys.* **2014**, *16*, 15278.
[46] M. Mateos, M.-D. Tchangaï, R. Meunier-Prest, O. Heintz, F. Herbst, J.-M. Suisse, M. Bouvet, *ACS Sens.* **2019**, *4*, 740.
[47] S. A. Alkaitis, G. Beck, M. Graetzel, *J. Am. Chem. Soc.* **1975**, *97*, 5723.
[48] M. Vizuete, M. J. Gómez-Escalonilla, S. García-Rodriguez, J. L. G. Fierro, P. Atienzar, H. García, F. Langa, *Chem. - Eur. J.* **2012**, *18*, 16922.
[49] M. Alvaro, P. Atienzar, P. De La Cruz, J. L. Delgado, H. Garcia, F. Langa, *J. Phys. Chem. B* **2004**, *108*, 12691.
[50] M. Alvaro, C. Aprile, P. Atienzar, H. Garcia, *J. Phys. Chem. B* **2005**, *109*, 7692.
[51] H. G. Baldoví, B. Ferrer, M. Álvaro, H. García, *J. Phys. Chem. C* **2014**, *118*, 9275.
[52] M. Lamblin, L. Nassar-Hardy, J.-C. Hierso, E. Fouquet, F.-X. Felpin, *Adv. Synth. Catal.* **2010**, *352*, 33.
[53] M. Blanco, B. Nieto-Ortega, A. De Juan, M. Vera-Hidalgo, A. López-Moreno, S. Casado, L. R. González, H. Sawada, J. M. González-Calbet, E. M. Pérez, *Nat. Commun.* **2018**, *9*, 2671.
[54] D. Mosconi, M. Blanco, T. Gatti, L. Calvillo, M. Otyepka, A. Bakandritsos, E. Menna, S. Agnoli, G. Granozzi, *Carbon* **2019**, *143*, 318.
[55] D. A. Nicewicz, D. W. C. Macmillan, *Science* **2008**, *322*, 77.
[56] D. González-Muñoz, A. Martín-Somer, K. Strobl, S. Cabrera, P. J. De Pablo, S. Díaz-Tendero, M. Blanco, J. Alemán, *ACS Appl. Mater. Interfaces* **2021**, *13*, 24877.